Journal of Sound and Vibration (1997) **205**(1), 103–111

LETTERS TO THE EDITOR

EMPLOYING FLUID FLOW IN A CANTILEVER PIPE FOR VIBRATION CONTROL

S. E. Semercigil, Ö. F. Turan and S. Lu†

Department of Mechanical Engineering, Victoria University of Technology, Footscray Campus, PO BOX 14428, *MCMC Melbourne, Victoria* 8001, *Australia*

(*Received* 17 *July* 1992, *and in final form* 5 *February* 1997)

1. INTRODUCTION

The subject of pipes conveying fluid has been studied extensively in the literature. Numerous reports on the topic have been published, including the two well recognized texts on flow induced vibrations [1, 2], each devoting one chapter to this subject. A relatively recent review is also given by Païdoussis [3]. Although the damping effect of the Coriolis force has long been recognized, past studies have concentrated mainly on the stability analysis. Only in one of the early works on this subject, Long examined the damping effect of the Coriolis force on the cantilever pipe both theoretically and experimentally [4]. Long's results were only for a limited set of flow parameters.

Due to the presence of the Coriolis force of the fluid, pipes conveying fluid may lose stability at high flow velocities. However, the same Coriolis force may have significant damping effect for a cantilever pipe at moderate flow velocities. This damping effect may be exploited to control the vibration of a light, resonant structure, if the pipe carrying the fluid is used as a controller. Of course, provisions must be made to collect and to re-circulate the working fluid if an unlimited source is unavailable.

In this study, the possibility of using the Coriolis effect as a vibration controller is demonstrated. In the following, the governing equation of motion and the numerical scheme are summarized. Then representative numerical results are presented. Finally, experimental observations are compared with those of the numerical simulations.

2. EQUATION OF MOTION AND THE METHOD OF DISCRETIZATION

Fluid flow through a cantilever pipe at constant velocity is illustrated in Figure 1. The equation of motion for the transverse vibration of the pipe is given as

$$EI\frac{\partial^4 y^*}{\partial x^{*4}} + \rho A v^2 \frac{\partial^2 y^*}{\partial x^{*2}} + 2\rho A v \frac{\partial^2 y^*}{\partial x^* \partial y^*} + c\frac{\partial y^*}{\partial t^*} + m\frac{\partial^2 y^*}{\partial t^{*2}} = 0. \tag{1}$$

Here, EI is the bending stiffness of the pipe; ρA, mass of the fluid per unit length; v, constant flow velocity in the pipe; m, combined fluid-pipe mass per unit length; and c is the viscous damping coefficient of the pipe. x^* and y^* are the axial distances along the pipe and the transverse displacement of the pipe, respectively, while t^* represents time.

The flow is assumed to be inviscid and incompressible plug flow. In most practical cases, the flow is fully turbulent with a fairly full mean velocity profile and negligible contribution of the fluid viscosity. The equation certainly does not account for any turbulence effects.

The equation of motion can be non-dimensionalized by substituting

$$y = y^*/l, \quad x = x^*/l, \quad t = t^*\sqrt{EI/ml^4},$$

† Now with the Department of Mechanical Engineering, University of California, Berkeley.

0022–460X/97/310103 + 09 $25.00/0/sv970987

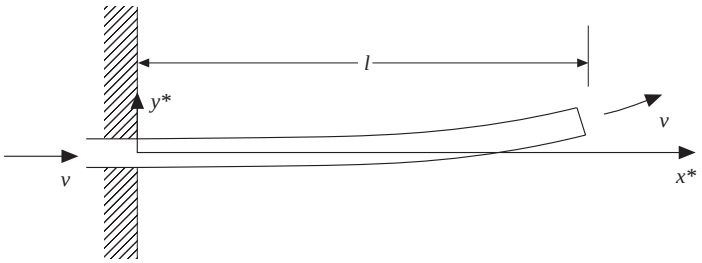

Figure 1. Fluid-conveying cantilever pipe.

where l is the pipe length. The resulting equation then becomes

$$\underbrace{\frac{\partial^4 y}{\partial x^4}}_{\text{(I)}} + \underbrace{V^2 \frac{\partial^2 y}{\partial x^2}}_{\text{(II)}} + \underbrace{2\sqrt{\beta} V \frac{\partial^2 y}{\partial x\, \partial t}}_{\text{(III)}} + \underbrace{D \frac{\partial y}{\partial t}}_{\text{(IV)}} + \underbrace{\frac{\partial^2 y}{\partial t^2}}_{\text{(V)}} = 0, \tag{2}$$

where $\beta = \rho A/m$, $V = vl\sqrt{\rho A/EI}$ and $D = cl^2/\sqrt{mEI}$.

Terms (I) and (V) constitute the simple beam equation, while (II) and (III) are the curvature term (or the centrifugal force term) and the Coriolis force term, respectively. Term (IV) in equation (2) represents the structural damping. The effect of the flow is reflected by parameters β and V. β is the ratio of fluid mass to the combined mass of the fluid and the pipe. V is the non-dimensional flow velocity.

In the first bending mode of a cantilevered beam, the gradient of the mode shape along the pipe is monotonous. Hence, $\partial^2 y/\partial x\, \partial t$ in the Coriolis term has the same direction as $\partial y/\partial t$. Therefore, the Coriolis force opposes the motion over the entire span of the pipe and behaves similarly to a viscous damping force. The dissipative effect of the Coriolis force forms the basis of this particular study. It should be remembered that the following discussion is valid for a cantilevered beam, and only in the fundamental mode. When the gradient of the deflected beam changes along the length, the damping effect becomes less significant [1, 2].

Boundary conditions to complement the equation of motion for the cantilever pipe are

$$\begin{aligned} &y(0, t), \qquad y'(0, t) = 0, \qquad \text{at the clamped end;} \\ &y''(1, t) = 0, \qquad y'''(1, t) = 0, \text{at the free end,} \end{aligned} \tag{3}$$

where primes represent a derivative with respect to the space variable x.

Here, a finite difference method is applied directly to the equation of motion. Terms in equation (2) involving only the time or spatial derivatives with even order are approximated with central difference:

$$\left(\frac{\partial^2 y}{\partial t^2}\right)_n^i = \frac{y_n^{i+1} - 2y_n^i + y_n^{i-1}}{\Delta t^2}, \qquad \left(\frac{\partial^2 y}{\partial x^2}\right)_n^i = \frac{y_{n+1}^i - 2y_n^i + y_{n-1}^i}{\Delta x^2},$$

$$\left(\frac{\partial^4 y}{\partial x^4}\right)_n^i = \frac{y_{n+2}^i - 4y_{n+1}^i + 6y_n^i - 4y_{n-1}^i + y_{n-2}^i}{\Delta x^4}.$$

For simplicity, backward difference with respect to time is used for the other terms:

$$\left(\frac{\partial y}{\partial t}\right)_n^i = \frac{y_n^i - y_n^{i-1}}{\Delta t}, \qquad \left(\frac{\partial^2 y}{\partial x\,\partial t}\right)_n^i = \frac{(y_{n+1}^i - y_{n-1}^i) - (y_{n+1}^{i-1} - y_{n-1}^{i-1})}{2\Delta x\,\Delta t}.$$

In these discretized forms, a superscript indicates time step and a subscript indicates spatial node. Substituting these finite difference approximations into equation (2) yields the discretized equation at the ith time step and nth spatial node as

$$\begin{aligned} y_n^{i+1} = {} & 2y_n^i - y_n^{i-1} - (\Delta t/\Delta x^2)^2(y_{n+2}^i - 4y_{n+1}^i + 6y_n^i - 4y_{n-1}^i + y_{n-2}^i) \\ & - V^2(\Delta t/\Delta x)^2(y_{n+1}^i - 2y_n^i + y_{n-1}^i) - \sqrt{\beta}V(\Delta t/\Delta x)(y_{n+1}^i - y_{n-1}^i - y_{n+1}^{i-1} + y_{n-1}^{i-1}) \\ & - D\,\Delta t(y_n^i - y_n^{i-1}). \end{aligned} \tag{4}$$

In addition, the discretized boundary conditions given by equation (3) become

$$y_0^i = 0, \qquad y_{-1}^i = 0, \qquad y_{N+1}^i = 2y_N^i - y_{N-1}^i, \qquad y_{N+2}^i = 4y_N^i - 4y_{N-1}^i + y_{N-2}^i, \tag{5}$$

where N is the total number of short segments into which the pipe is discretized. $N = 40$ is used in the simulations. This simple explicit method is conditionally stable when $\Delta t/\Delta x^2 < 0{\cdot}5$ for the simple beam equation [5]. Due to the two additional fluid terms and backward differencing with respect to time, $\Delta t/\Delta x^2 = 0{\cdot}01$ is used during computations to ensure numerical stability.

3. NUMERICAL RESULTS

To initiate oscillations, an initial distributed velocity was imposed, starting from the position of rest. In order to avoid the contribution of the higher modes, the distribution of this initial velocity was set to be the same as the fundamental mode.

In Figures 2 and 3, typical tip displacement histories of the cantilevered pipe are given for different volumetric flow rates, Q. The displacement is non-dimensionalized by dividing with the peak displacement amplitude of the case without flow (uncontrolled), Y_0. The structural parameters in these two figures are the same as those used in the experimental observations, and they are listed in Table 1. Figure 2 represents the PVC pipe alone; whereas the results in Figure 3 are for the case when the same PVC pipe was used as the vibration controller alongside a copper pipe.

In Figure 2(a), the no-flow case represents the solution of the standard beam equation. For this case, the rate of attenuation is quite low, due to very light inherent structural damping. As the flow rate increases, however, the rate of attenuation improves dramatically. As discussed earlier, this improvement is caused by the Coriolis force whose amplitude is proportional to the fluid velocity.

Figure 3 shows the displacement histories when the PVC pipe of Figure 2 was used as a controller, as mentioned earlier. The structure to be controlled was another cantilevered pipe, attached along the length of the fluid-carrying pipe. Hence, only the structural mass and stiffness parameters were changed in the simulations to generate the results in Figure 3. For the cases where the structure to be controlled is not as simple, this treatment is expected to be more involved. However, the treatment of the fluid-carrying pipe dynamics remains the same.

With increasing Q, improvement of the attenuation rates in Figure 3 is not as drastic as that in Figure 2. The reason for this change is due to the increase in the structural mass to be controlled as compared to the mass of the fluid. The mass ratio, β, decreases to 0·25

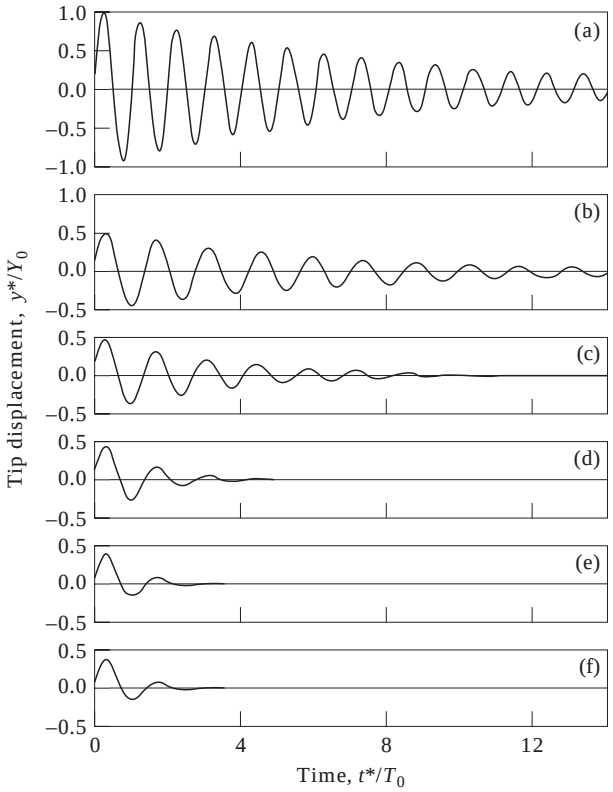

Figure 2. Tip displacement histories for different flow rates (Q l/min) of (a) Q = 0; (b) 4·8; (c) 15·0; (d) 40·0; (e) 64·4 and (f) 75·0. y^* transverse displacement; Y_0 uncontrolled peak displacement; t^* time; T_0 uncontrolled fundamental period.

in Figure 3 from 0·49 in Figure 2. The effect of the mass ratio β and the flow velocity will be investigated next.

Figure 4 shows the effect of the mass ratio, β, on the effectiveness of control. The parameter R of the vertical axis represents the ratio of the second peak displacement amplitude (positive) to that of the first. Hence, a small R indicates effective control. Values of R are shown for different velocities V of up to 2·0, where the critical velocity at low

TABLE 1

Parameters of the experimental structures. Length l, outer diameter o.d. and thickness are in mm. m_{eq}, k_{eq} and ζ_{eq} represent the equivalent mass, stiffness and the critical damping ratio at the free tip, and in the fundamental mode

Material	Dimensions ($l \times$ o.d. $\times$ thick.)	Natural† freq. (Hz)	k_{eq}‡ (N/m)	m_{eq}‡ (kg)	ζ_{eq}‡
PVC	1740 × 19 × 3·2	1·60 ± 0·05	20·1	0·14	0·025 ± 0·005
PVC and copper	1740 × 19 × 3·2 and 1740 × 10 × 1·6	4·50 ± 0·02	370·2	0·40	0·019 ± 0·008

† Measured ‡ Calculated

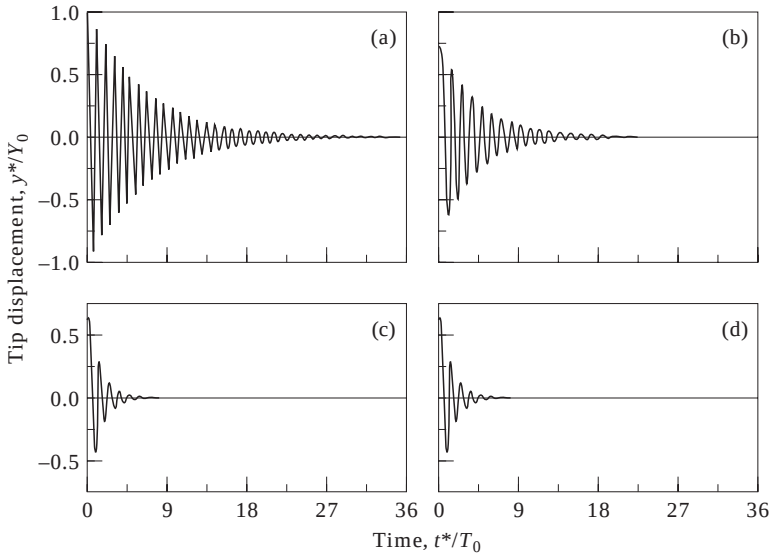

Figure 3. Tip displacement histories for different flow rates (Q *l*/min) of (a) 0; (b) 24·93; (c) 132·74 and (d) 180·54. Format is the same as in Figure 2.

mass ratios is about 4 as the limit of stable oscillations [5]. There is no structural damping, $c = 0$, in these cases.

In Figure 4, at relatively high flow velocities (of $V = 0{\cdot}5$ and larger), the effectiveness of damping increases quite rapidly with the mass ratio β (for β of about 0·2 and smaller). For larger β, the change in R becomes more gradual with increasing β. Hence, for high flow velocities, the effect of increasing mass ratio diminishes, as the mass ratio increases. The value of R is zero for $\beta = 0{\cdot}4$ and larger and for $V = 2{\cdot}0$, since a second peak is not attainable due to the effectiveness of the control.

Figure 5 shows the effectiveness of the control on the ratio, Y_p, of the peak displacements with flow to without flow. The results in Figures 4 and 5 are closely related. With the exception of the lower right part in Figures 4 and 5 (where β and V are both high and there is a significant departure in frequency of oscillations from the no flow case), it is

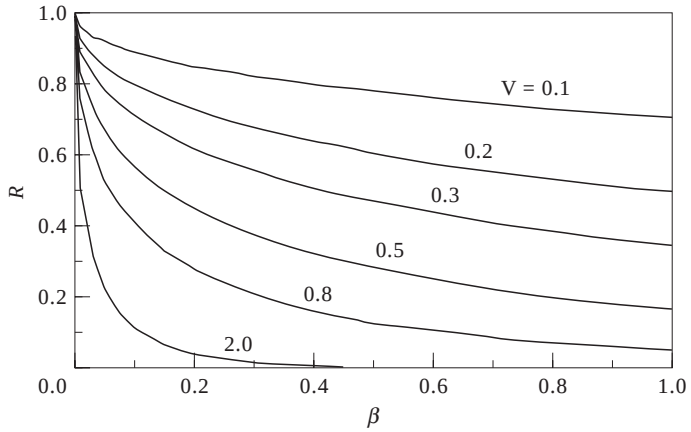

Figure 4. Variation of R with β for different flow velocities V.

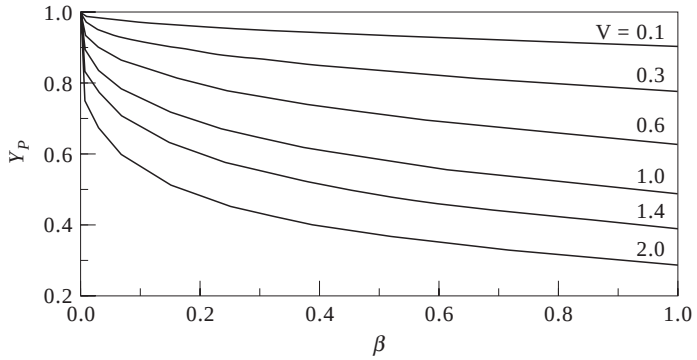

Figure 5. Variation of Y_p with β for different flow velocities V.

found that $R \cong Y_p^4$. Since the initial conditions are the same for all cases, and there is no damping in the no-flow case, Y_p is simply the decay of the exponential envelope in about the first 1/4 period, and R in one period.

4. EXPERIMENTS

Experiments were designed to check the validity of the computational results. The experimental setup is shown in Figure 6. The rig was a closed loop including a large reservoir, a circulating pump, piping and a pair of valves to regulate the volumetric flow rate. Water was used as the working fluid. A steel tank of 1·04 m by 1·01 m cross-section and 0·73 m depth was used as a reservoir. An in-line pump with a head of 36·6 m (120 ft) at 1·78 m^3/min (470 gal) was used to provide circulation. Cast iron pipes of 77 mm (3 in) diameter were used until the point where a PVC flexible pipe of 19 mm (0·75 in) diameter was attached. The cast iron pipe was fixed on a wall (approximately 3·5 m) and across the ceiling (approximately 2 m) over the reservoir. Three standard 90° elbows were used to accomplish the direction changes. Piping was clamped on the wall and the ceiling at four different locations to ensure structural integrity. The parameters of the fluid-carrying PVC pipe and the copper pipe to be controlled are given in Table 1.

An open jet of water was formed at the free tip of the PVC pipe which was collected in the reservoir and circulated. The volume flow rate was recorded by immersing a 60 liter

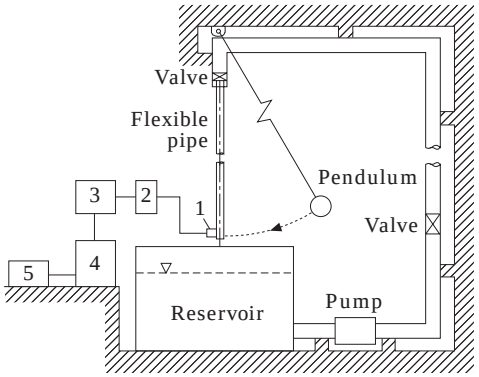

Figure 6. Experimental setup. 1, Bruel and Kjaer accelerometer type 4332; 2, Bruel and Kjaer amplifier, type 2625; 3, Rockland filter set, model 432; 4, Nicolet oscilloscope, model M20X1; 5, Hewlett Packard plotter, model 7470A.

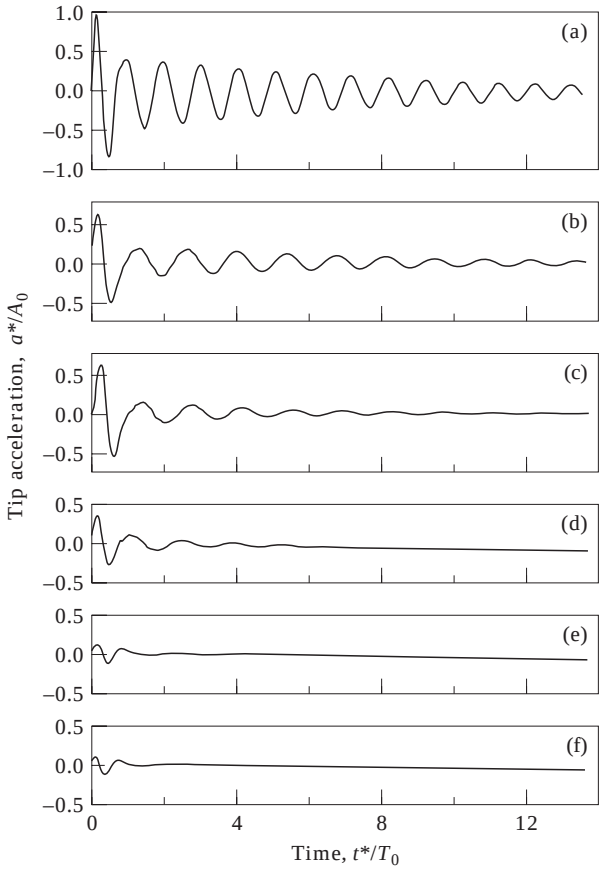

Figure 7. Tip acceleration histories for different flow rates (Q *l*/min) of (a) 0; (b) 4·8; (c) 15·0; (d) 40·0; (e) 64·4 and (f) 75·0. Format is the same as in Figure 2, but a^*: transverse acceleration; A_0: uncontrolled peak acceleration.

container in the reservoir and recording the time required to fill this container at different valve openings. Repeated flow rate measurements showed a variation well within $\pm 5\%$ of the nominal values reported here. The experimental procedure consisted of exciting the pipe by striking it at the tip with a pendulum which was suspended from the ceiling. The pendulum was used to provide a repeatable transient disturbance to the pipe, by releasing it from the same horizontal distance. Care was taken to avoid multiple strikes during the tests.

The response of the PVC pipe was measured by using an accelerometer, Item 1 in Figure 6. The output of the accelerometer was first amplified and filtered to avoid extraneous high frequency noise and the contribution of higher modes. The cut-off frequency of the low pass filter was set to be at least twice as large as the fundamental frequency of the pipe. A digital oscilloscope was used to capture the history of the acceleration. A hard copy was obtained with an X-Y plotter, when needed.

The acceleration histories of the tip of the PVC pipe are shown in Figure 7, for different flow rates, Q, ranging from 0–75 l/min. The acceleration is non-dimensionalized by dividing with the peak acceleration amplitude of the case without flow (uncontrolled), A_0. The case without flow shows the natural vibrations of the pipe with a very light inherent structural damping. This case shows an almost identical trend, starting from the second

cycle, to that of the computational case in Figure 2. However, the first cycle has an unexpectedly large peak amplitude and a shorter period than the following cycles. It is believed that this is due to the contribution of the higher structural modes. Since the transient disturbance is of impulsive type, it is expected that the higher structural modes of the pipe be excited along with the fundamental mode. Although the acceleration signal was filtered to observe the natural vibrations at the fundamental mode only, it is practically impossible to entirely exclude the contribution of high frequencies. In addition, measuring the acceleration rather than the displacement further exaggerates the high frequency contribution.

The same trend of having the first cycle with a larger peak amplitude and a shorter period may be observed for the other flow rates in Figure 7. Although the general trend is quite consistent with the numerical simulations shown in Figure 3, experimental measurements show a more drastic attenuation of the peak response for any given flow rate. Hence, an energy dissipation mechanism, which is effective at higher frequencies, plays an important role in the experiments which is not accounted for in the numerical simulations. It may be argued that this difference between the numerical simulations and the experimental measurements is due to the plug flow assumption used in the derivation of the equation of motion for the pipe. Considering that the measurements involved Reynolds numbers of up to $1{\cdot}9 \times 10^5$, based on the pipe diameter, dissipative mechanisms due to the time-variant components of the flow may have an effect.

Results shown in Figure 8 correspond to the case when another flexible copper pipe was cantilevered from the same rigid base as the fluid-carrying PVC pipe. The PVC pipe was securely attached to the copper beam with hose clamps. Hence, the damping effect of the flow through the PVC pipe was employed to control the combined structure this time. When the results in Figure 8 are compared to those of the numerical simulations shown in Figure 3, a similar trend may be observed to that between Figures 2 and 7. Experimental measurements show a different behavior at the beginning of the oscillations and larger attenuations are obtained in the oscillation amplitudes as compared to the numerical results. Except for these differences, there is close similarity between the experiments and simulations. Therefore, experimental measurements show an at least as effective control of transient vibrations as the numerical predictions.

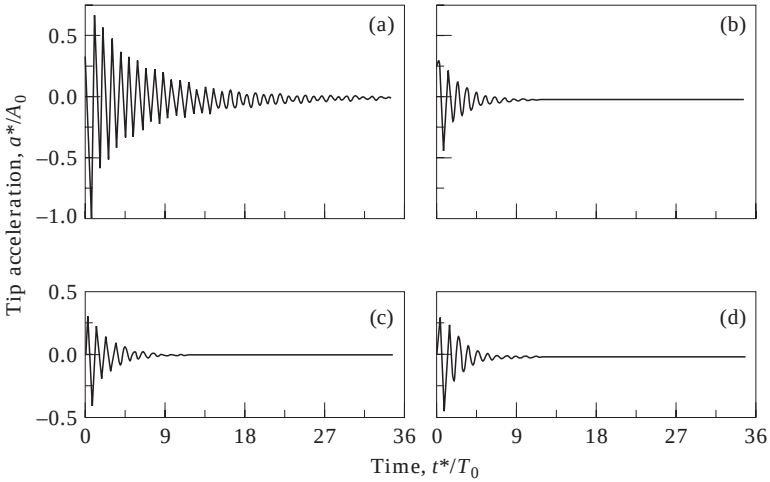

Figure 8. Tip acceleration histories of the controller pipe for different flow rates (Q *l*/min) of (a) 0; (b) 24·93; (c) 132·74 and (d) 180·54. Format is the same as in Figure 7.

5. CONCLUSIONS

The transient vibration of a fluid-conveying cantilever pipe is simulated numerically by using a simple finite difference scheme. Both experimental results and numerical simulations suggest that the damping of the flow in a cantilever pipe can be effective, and may have potential in engineering applications as a controller. Design charts are provided to indicate the important flow parameters to enhance the vibration attenuation characteristics.

REFERENCES

1. R. D. Blevins 1990 *Flow Induced Vibration*. New York: Von Nostrand Reinhold, second edition.
2. S. S. Chen 1987 *Flow-induced Vibration of Circular Cylindrical Structures*. Hemisphere Publishing Corporation.
3. M. P. Païdoussis 1991 *Proceedings of the Canadian Society of Mechanical Engineers*, **2,** 1–33. Pipes conveying fluid: a model dynamical problem.
4. R. H. Long, Jr. 1955 *Journal of Applied Mechanics* **22**, 65–68. Experimental and theoretical study of transverse vibration of a tube containing flowing fluid.
5. W. F. Ames 1969 *Numerical Methods in Partial Differential Equations*, 273–275. New York: Barnes & Noble.
6. R. W. Gregory and M. P. Païdoussis 1966 *Proceedings of the Royal Society* A **293**, 512–527. Unstable oscillation of tubular cantilevers conveying fluid. I. Theory.